energies

MDPI

Article

Automatic Resonance Tuning Technique for an Ultra-Broadband Piezoelectric Energy Harvester

Sallam A. Kouritem [1,*], Muath A. Bani-Hani [2], Mohamed Beshir [3], Mohamed M. Y. B. Elshabasy [1,4] and Wael A. Altabey [1,5,*]

1 Department of Mechanical Engineering, Faculty of Engineering, Alexandria University, Alexandria 21544, Egypt
2 Department of Aeronautical Engineering, Jordan University of Science and Technology, Irbid 22110, Jordan
3 School of Engineering, University of Edinburgh, Edinburgh EH8 9YL, UK
4 Department of Mechanical and Manufacturing Engineering, Jubail Industrial College, Male Branch, Al Jubail 35718, Saudi Arabia
5 International Institute for Urban Systems Engineering (IIUSE), Southeast University, Nanjing 210096, China
* Correspondence: sallam.kouritem@alexu.edu.eg (S.A.K.); wael.altabey@gmail.com (W.A.A.)

Abstract: The main drawback of energy harvesting using the piezoelectric direct effect is that the maximum electric power is generated at the fundamental resonance frequency. This can clearly be observed in the size and dimensions of the components of any particular energy harvester. In this paper, we are investigating a new proposed energy harvesting device that employs the Automatic Resonance Tuning (ART) technique to enhance the energy harvesting mechanism. The proposed harvester is composed of a cantilever beam and sliding masse with varying locations. ART automatically adjusts the energy harvester's natural frequency according to the ambient vibration natural frequency. The ART energy harvester modifies the natural frequency of the harvester using the motion of the mobile (sliding) mass. An analytical model of the proposed model is presented. The investigation is conducted using the Finite Element Method (FEM). THE FEM COMSOL model is successfully validated using previously published experimental results. The results of the FEM were compared with the experimental and analytical results. The validated model is then used to demonstrate the displacement profile, the output voltage response, and the natural frequency for the harvester at different mass positions. The bandwidth of the ART harvester (17 Hz) is found to be 1130% larger compared to the fixed resonance energy harvester. It is observed that the proposed broadband design provides a high-power density of 0.05 mW mm^{-3}. The piezoelectric dimensions and load resistance are also optimized to maximize the output voltage output power.

Keywords: piezoelectric energy harvesting; broad bandwidth; automatic resonance tuning; FEM

Citation: Kouritem, S.A.; Bani-Hani, M.A.; Beshir, M.; Elshabasy, M.M.Y.B.; Altabey, W.A. Automatic Resonance Tuning Technique for an Ultra-Broadband Piezoelectric Energy Harvester. *Energies* **2022**, *15*, 7271. https://doi.org/10.3390/en15197271

Academic Editors: Abdessattar Abdelkefi and Enrique Romero-Cadaval

Received: 16 August 2022
Accepted: 29 September 2022
Published: 3 October 2022

1. Introduction

Researchers and industries have been interested in piezoelectric energy harvesting due to its great ability to provide self-powered electronic wearable devices, wireless sensor networks, and medical implants. Piezoelectric energy converts mechanical energy to electricity with high efficiency and ease of operation. The harvested power can be employed in many medical and industrial applications such as pacemakers, bridges, building monitoring, and tire pressure monitoring techniques [1]. Many energy sources can be harvested using a piezoelectric device such as wasted mechanical vibrations energy from buildings, bridges, structures, and vehicles [1,2]. Unlike other energy conversion methods, the mechanical energy harvesting technique is not influenced by outdoor or indoor surroundings circumstances and can operate under various circumstances. Many devices can convert mechanical energy into electrical energy using piezoelectric [3], electromagnetic [4], and electrostatic [5] energy. Due to their integrity with the vibrating platform, high efficiency, and high-power density, piezoelectric energy harvesting devices were widely investigated [6–8].

To maximize the generated electrical power from mechanical sources, the piezoelectric energy cantilever should be designed to operate at its fundamental resonance frequency. Typically, piezoelectric harvesters exhibit a narrowband response around the resonance frequency. Therefore, it is highly desirable to build piezoelectric energy harvesters that can work under wide broadband mounting conditions and dynamics. Thus, the harvester's natural frequency should resonate with the excitation frequency of the ambient vibration to maximize the harvested output power and enhance the bandwidth of the natural frequency under practical conditions. One way to do that is by employing a mechanical structure or dedicated electronics to adjust the harvester's natural frequency, which results in additional implementation difficulties [1]. Therefore, it is very necessary to propose an energy harvester with an adaptable natural frequency that matches the surrounding resonance frequencies.

Many broadband energy harvesting techniques have been introduced in the literature. Few used the nonlinear properties of the structural stiffness and others used the effect of an external magnetic force [9–11]. However, minor enhancement in natural frequency bandwidth was achieved at the expenses of the size of the harvester, the size of the proof mass, and the external magnet. Graded resonance frequencies were used as well. This technique gave a low energy density due to the fact that only one harvester in the array can work at a given frequency [12–14]. Another way used to enhance the frequency bandwidth was the active resonance tuning method by using sensors that could detect the resonance then, the controllers actively adjusted the natural frequency by changing the stiffness. The disadvantage of this technique was the additional energy requirement which decreases the total net output power, and in some cases, the required power was larger than the power harvested [15].

The harvesters' modelling, design, structures, and maximizing of their output power were introduced by [16–18]. C. Lu et al. [16] introduced a distinctive Maximum Power Point tracking system to increase the output power from the vibration harvester. Mohamed et al. [17] introduced a shape optimization methodology of five different shapes of harvesters numerically using COMSOL and analytically using a Genetic Algorithm to maximize the output power. Wang et al. [18] proposed a technique that depends on the vibrations through a covering extractor and then adapts the rectified voltage to reach the highest output power. The harvester parameters are optimized here in our research similar to the iterative(systematic) optimization technique utilized in literature research [19–23]. Jian et al. [24] introduced a technique of broadband vibration drop using a graded piezoelectric metamaterial harvester. Wang et al. [25] proposed a smart piezoelectric energy harvester to widen the natural frequency. Bani-Hani et al. [26] proposed a self-powered sensor that includes 17 harvesters to sense the Earthquake- structural vibration in the wideband range (1-17 Hz) Staaf et al. [27] enhanced bandwidth by self-tuning through irregular planning and extra sliding mass. Rui et al. [28,29] presented a passive self-tuning harvester for wideband achieved by centrifugal effect in the rotational structures. Kouritem [30] showed the effect of the second mode vibrations and concentrated masses on an array of harvesters. Additionally, the effect of various materials on an array of harvesters' performance is investigated. Kouritem et al. [31] introduced an excellent broadband technique by adjusting the tip masses angle of five beams. The problem of lowering the power between the peaks was completely solved using the proposed technique. In addition, the effect of harvester parameters on the output power and broadband width were further investigated. Silveira et al. [32] proposed an energy harvester to harvest the vibrational energy of tilting pad journal bearing. In their work, they described the influence of n-vibrational modes. Liu et al. [33] presented a wideband natural frequency method (a tri-stable mechanism) using four springs coupled with a constructed structure, which has a larger stroke.

In this research, an automatic resonance tuning (ART) is demonstrated numerically to control the natural frequency of the designed harvester. The ART harvester adapts its natural frequency related to the vibration source excitation frequency without the need for external power. The ART cantilever changes the natural frequency based on

the position of a proof mass on a cantilever beam. The mobile (sliding) mass can change its position over the oscillating cantilever beam. The mobile mass moves on a vibrating cantilever beam (low friction condition) to track the resonance position and then it stops due to the high friction to obtain the exact source frequency. This technique is denoted by resonance conditioning. The mass then moves again due to changing the source frequency (off-resonance condition). A similar work has been investigated by using a self-tuning phenomenon. For example, Babitsky and Veprik [34] presented a self-tuning method consisting of a sliding washer on a beam to decrease the dynamic response of a beam to the impulsive excitation. Thomsen [35] studied numerically and analytically the self-damping device. Moreover, Miller et al. recorded an experimentally passive self-tuning system for a beam resonator with a sliding mass [36]. Designing a harvester with a frequency of less than 30Hz is a great challenge. The natural frequencies of MEMS are usually larger than 1 kHz [37,38]. Nevertheless, the surrounding ambient vibration frequencies exist in broadband and low frequency. Thus, the main contribution of our research is to construct a harvester that works over low frequency and natural broadband frequencies that can achieve a high-power density as well. However, to the knowledge of the author, there is no work for a harvester (cantilever beam) for broadband frequency and high-power density without needing an extra device that is employed in similar techniques such as with magnets, springs, stoppers, or an array of cantilevers (large dimensions). The proposed technique can be considered a smart solution that overcomes many challenges in the field of broadband energy harvesting. To describe the ART energy cantilever utilized for low and wideband natural frequency, the cantilever displacement profile is investigated in this work at different mass positions using FEM. In addition, we simulate the voltage response of the piezoelectric cantilever corresponding to the mass position. Furthermore, we optimize the piezoelectric patch parameters such as length and thickness. Finally, the analytical and experimental validation studies are performed to validate the proposed FE model. The FEM model is also validated using three previously published experimental results in the same area. We aim to harvest energy form the vibration of bridges and buildings of a wide frequency range (5–22 Hz) [31,39] and then use the harvested power in condition monitoring (see Figure 1).

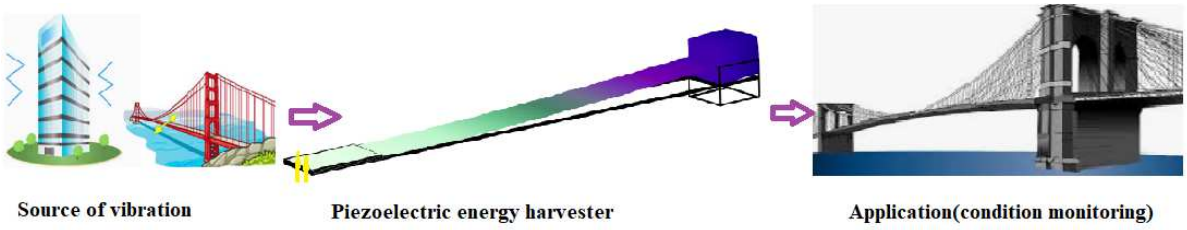

Figure 1. Energy harvesting from vibrations of bridges and buildings used in condition. Monitoring.

2. Analytical Model of Harvester

A piezoelectric energy harvester composed of a cantilever beam with a proof mass is schematically shown in Figure 2a. As the first mode introduces a great part of the energy, we only consider the fundamental mode (first mode) [40], since the fundamental excitation mode provides more than 81% of the total energy [17]. Thus, the harvester is modeled as a single degree of freedom (SDOF) as shown by Figure 2b.

The equation of motion for the simplified single degree of freedom model can be expressed as [41]:

$$(m_h + M)\ddot{y} + c_h\dot{y} + k_h y - \theta v = -(\mu + M)\ddot{y}_b \quad (1)$$

$$C_p\dot{v} + \frac{v}{R_l} + \theta\dot{y} = 0 \quad (2)$$

where M is tip mass, y_b is the base excitation at the fixed end, y is the relative displacement of the free end relative to the base, v the output voltage, k_h the stiffness of the harvester, c_h is the damping coefficient, m_h is the equivalent mass of the harvester at the free end, C_p is the

piezoelectric capacitance, R_l is the external resistance, θ is the mechanical-electrical coupling coefficient, and μ is the equivalent inertia of the harvester relative to base excitation.

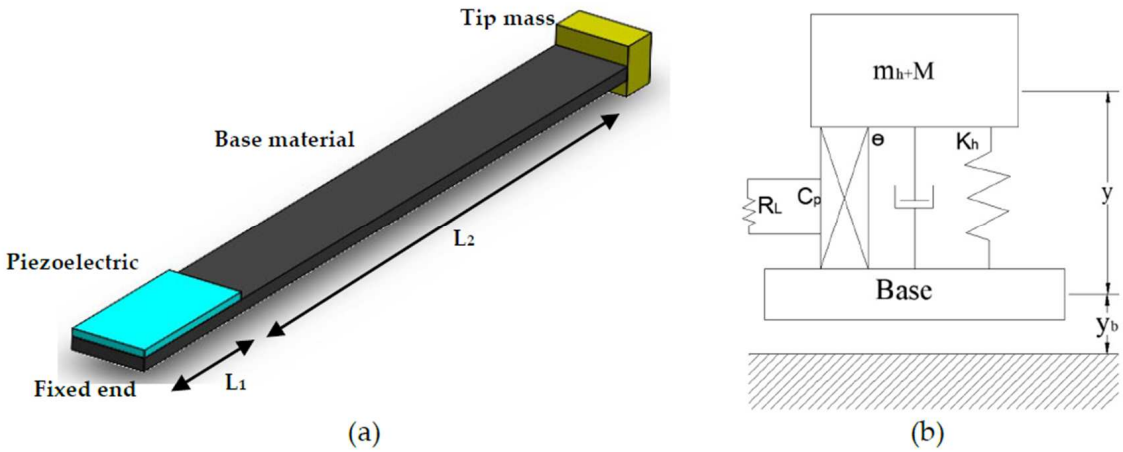

Figure 2. (**a**) The diagram of the piezoelectric harvester with tip mass; (**b**) the simplified single-degree model.

The steady-state solutions of Equations (1) and (2) under a harmonic excitation frequency ω are expressed as:

$$y = Ye^{i\omega t},\ v = Ve^{i\omega t},y_b = Y_b e^{i\omega t}, \tag{3}$$

$$\omega_n = \sqrt{\frac{k_h}{m_h + M}},\ \Omega = \frac{\omega}{\omega_n},\ \ \xi = \frac{c_h}{2m_h\omega_n}, \alpha = \omega_n c_p R_l, k^2 = \frac{\theta^2}{k_h\, c_p} \tag{4}$$

where ω_n is the natural frequency of the first mode, ξ is the damping ratio, Ω is the source (excitation) frequency, α is a time constant, and k^2 is an electromechanical coupling coefficient. Substituting Equations (3), and (4) into Equations (1) and (2), the voltage frequency response (V) can be derived as:

$$V = \frac{-i(\mu + M)\ \alpha\ \theta\ \Omega^3\ Y_b}{c_p(\mu + M)(1 + i\alpha\Omega + i\alpha\Omega k^2 + 2i\xi\Omega - \Omega^2 - 2\Omega^2\xi\alpha - i\alpha\Omega^3)}, \tag{5}$$

The proposed beam can be represented by segments (stepped beam). L_1 represents the composite segment of the beam with the active layer of PZT and the beam substructure. L_2 represents a single layer of the substructure of the beam. Therefore, the equivalent stiffness k_h and the equivalent mass m_h are defined in Equations (12) and (13). The transverse displacement, $y_i(x,t)$ of the stepped harvester can be expressed as:

$$y_n = w_n(x)e^{i\omega t}\ ,\ n = 1,\ 2 \tag{6}$$

where $w_i(x)$ is the modal function of the beam segments. The beam segment number is denoted by n, for a total of 2 segments. The equivalent kinetic energy T and the potential energy U for the simple degree of freedom model are expressed as:

$$T = \frac{m_h}{2}\left(\frac{\partial}{\partial t}(y_2\ (L_1 + L_2,\ t))\right)^2, \tag{7}$$

$$U = \frac{k_h}{2}(y_2\ (L_1 + L_2,\ t))^2. \tag{8}$$

The rigidity of the first beam segment, the distance from the bottom to the first composite beam segment to the neutral axis, and the rigidity of the second beam segment is expressed in [42]:

$$EI_1 = \frac{b}{6}\left(E_s\left(2\left(h_1^3\right) - 3y_0\left(h_1^2\right)\right) + E_p\left(2\left(h_2^3 - h_1^3\right) - 3y_0\left(h_2^2 - h_1^2\right)\right)\right) \tag{9}$$

$$y_0 = \frac{1}{2}\,\frac{E_s h_1^2 + E_p\left(h_2^2 - h_1^2\right)}{E_s h_1 + E_p(h_2 - h_1)} \tag{10}$$

$$EI_2 = \frac{E_s h_1^3 b}{12} \tag{11}$$

where, E_s and E_p are Young's modulus of the substrate material and the piezoelectric material, respectively. h_1, h_2, *and* b are the thicknesses of the substrate and the composite section (beam segment 1), and cantilever width, respectively. At this point, the equivalent stiffness k_h, equivalent mass m_h, electromechanical coupling coefficient θ, tip correction mass μ, and the capacitance of the piezoelectric material c_p are expressed as follows:

$$k_h = \frac{EI_1 \int_0^{L_1}\left(\frac{d^2 w_1(x)}{dx^2}\right)^2 dx + EI_2 \int_{L_1}^{L_1+L_2}\left(\frac{d^2 w_2(x)}{dx^2}\right)dx}{\left(W_2\left(L_1 + L_2,\, t\right)\right)^2} \tag{12}$$

$$m_h = \frac{\rho_1 \int_0^{L_1}(W_1(x))^2 dx + \rho_2 \int_{L_1}^{L_1+L_2}(W_2(x))^2 dx}{\left(W_2(L_1 + L_2,\, t)\right)^2} \tag{13}$$

$$\mu = \rho_1 \int_0^{L_1}(W_1(x))^2 dx + \rho_2 \int_{L_1}^{L_1+L_2}(W_2(x))^2 dx \tag{14}$$

$$\theta = e_{31} h_{pc} b \int_0^{L_1}\left(\frac{d^2 w_1(x)}{dx^2}\right)dx \tag{15}$$

$$c_p = \frac{e_{33}^s b L_1}{h_p} \tag{16}$$

where, ρ_1 is the mass density of the first beam segment, ρ_2 is the mass density of the second beam segment, h_{pc} is the distance from the neutral axis of the composite cross-section to the mid-height of the piezoelectric layer, and h_p is the thickness of the piezoelectric layer. To simplify the solution, the static deflection functions of the stepped cantilever beam subjected to a load (p) at the free end can be obtained. The static deflection of the first section, slope function, and static deflection of the second section are presented as:

$$w_1(x) = \frac{px^2}{6EI_1}\,(3L_1 - x) + \frac{pL_1 x^2}{2EI_1} \tag{17}$$

$$\theta_1(x) = \frac{d}{dx} w_1(x) \tag{18}$$

$$w_2(x) \;= w_1(L_1) \;+ \theta_1(x)(x - L_1) + \frac{p(x - L_1)^2}{6EI_2}(3L_2 - (x - L_1)) \tag{19}$$

We can evaluate the voltage from Equation (5) using the previous approximate modal functions. The harvester is subjected to a simple harmonic base excitation. In comparison to the previous work of Lee and Lin [40], where they used the static deflection functions for the analytical solution that yields minimum errors for small lengths of piezoelectric patches. Our analytical model is utilized for the purpose of validation of the FEM model. In future work, it is highly suggested that the analytical model will be developed for different positions for the mass along the beam.

3. Validation Study of FEM COMSOL Model

The COMSOL is commonly employed to simulate a real-life piezoelectric energy harvester. FEM COMSOL can be utilized for simulation in several research fields where it is hard to carry out a physical experiment or to develop an analytical model. Due to its high accuracy, it is extensively used by researchers. In piezoelectric energy harvesting, the COMSOL results were compared with analytical and experimental results in the literature [12,17,30,31,40]. Furthermore, it is employed in many studies in the literature to investigate the performance of harvesters. This has confirmed the convergence of the FEM analysis by COMSOL with the corresponding experimental and analytical ones and that let us be confident in our FEM results.

In this section, a comparison is conducted between our FEM model, and experimental and analytical literature results to validate our model. First, FEM results are compared to the experimental results of Shin et al. [43] which are based on the same ART phenomena. The properties and dimensions of the piezoelectric and subtract layers are the same as those given by reference [43] as shown in Table 1. The model of [43] is a completely clamped beam of two layers of PVDF (piezoelectric material) and spring steel.

Table 1. Material and geometric parameters of the harvester utilized for experimental validation.

Parameters	Steel	PVDF	Material	Steel	Piezoelectric
Length (mm)	90	90	Density (kg m^{-3})	7740	1700
Width (mm)	10	10	Young's modulus (GPa)	205	7.9
Thickness (mm)	0.2	0.11	Poisson's ratio	0.33	0.3
Tip mass (g)	1.84				

Figure 3 shows the natural (first mode) frequency calculated using the Eigen frequency study (COMSOL). Figure 4 reveals the comparison of the FEM COMSOL model results and the experimental results of reference [43], where the frequency position relation comparison is shown in Figure 4a and the voltage frequency relation is shown in Figure 4b. As shown in Figures 3 and 4, COMSOL overestimated the frequency and the position frequency relation by around +2.2% and +2.8 %, respectively, which gives a lot of confidence in using FEM in this study.

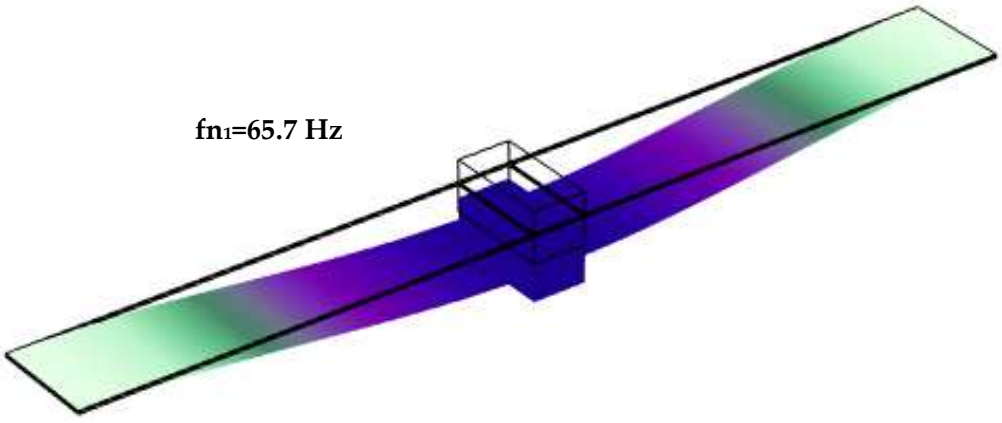

Figure 3. The first Eigen frequency of completely clamped beam.

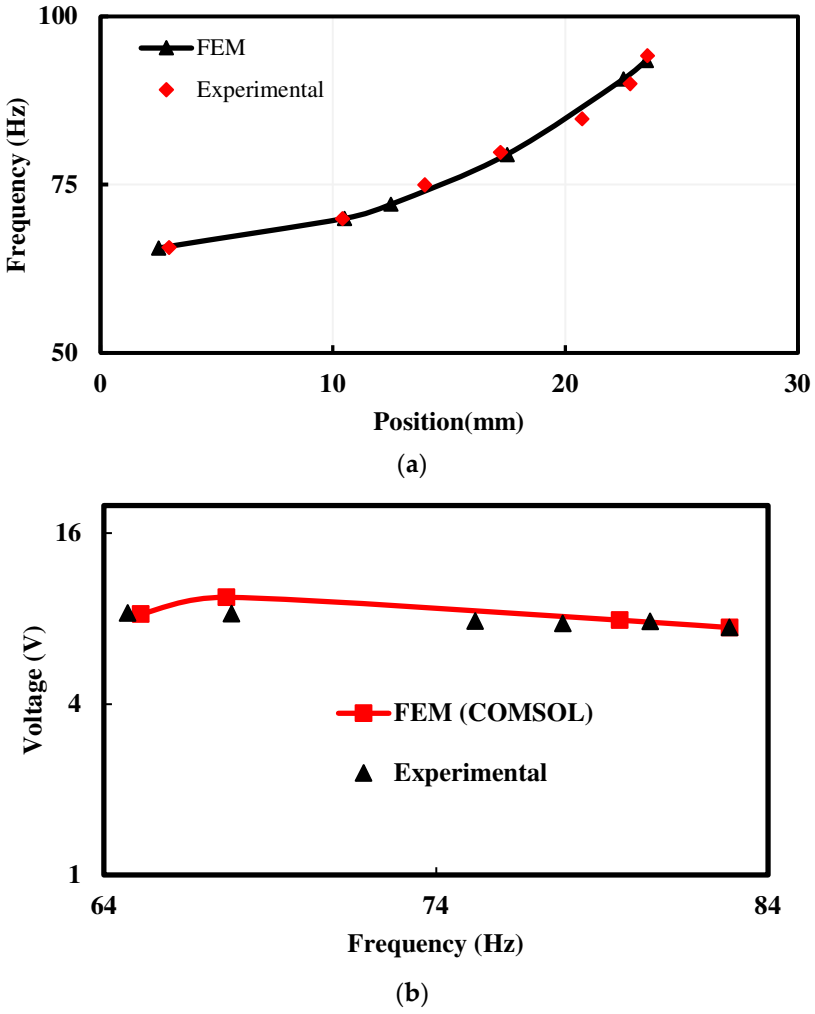

Figure 4. Comparison of the FEM COMSOL model results and the experimental results of reference [43]. (**a**) frequency position relation, (**b**) voltage frequency relation.

To demonstrate that the ART piezoelectric harvester can replace and outweigh the array harvester design, we first compare our FEM array model with the literature on two array harvesters. The first array COMSOL model is compared with the array harvester results of Yildirim et al. [12]. The first array is based on aluminum subtract material and consists of four cantilevers (see Figure 5). The mechanical properties of the subtract material are Young's modulus of 69.5 GPa, the density of 2700 kg/m^3, and Poisson's ratio of 0.33. Table 2 shows the parameters of the cantilevers: length (L), width (b), thickness (h), and tip mass. The utilized piezoelectric material is a macro fiber composite (MFC) (M-2807-P1). Table 3 shows the comparison between the natural frequency of FEA COMSOL and the experimental natural frequencies of the first array model. In addition, the results shown in Table 3 reveal good agreement between both the FEM and experimental results.

Table 2. The parameters of the cantilevers utilized for validation [12].

Beam	A	B	C	D
Length (mm)	165	165	165	165
Width (mm)	17.23	17.02	17.17	17.17
Thickness (mm)	0.6	0.6	0.6	0.6
Tip mass (g)	15.2	10.8	10.26	8.8

Table 3. Comparison between the natural frequency of FEA COMSOL and natural frequencies calculated experimentally by Ref. [12].

Beam	A	B	C	D
COMSOL natural frequency (Hz)	5.049	5.82	5.97	6.34
Experimental natural frequency (Hz)	5.3	5.45	5.6	6.39
Error %	4.73	6.35	6.1	0.78

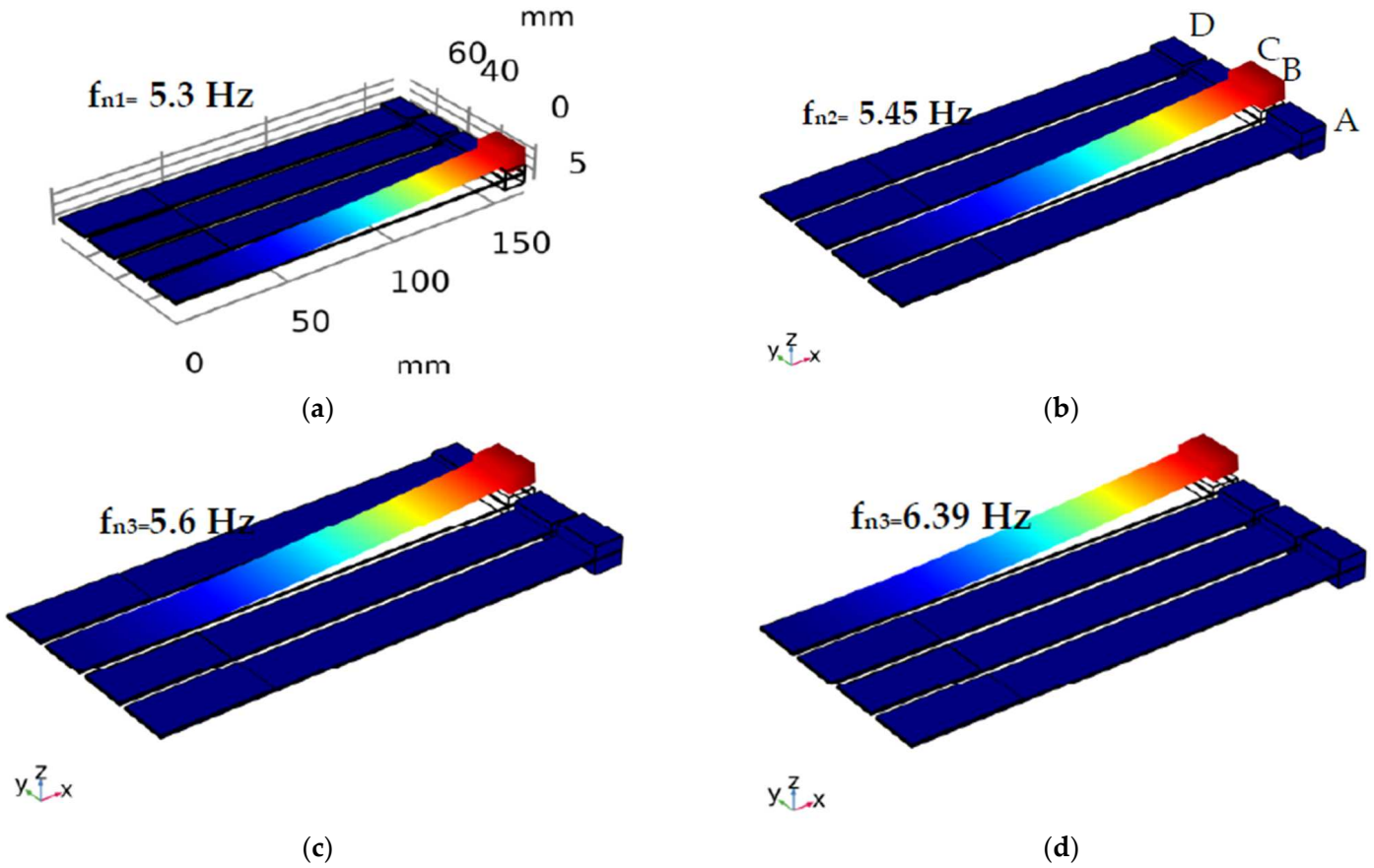

Figure 5. Natural frequencies of first array model. (**a**) natural frequency of beam A, (**b**) natural frequency of beam B, (**c**) natural frequency of beam C, and (**d**) natural frequency of beam D.

The second array COMSOL model is compared with the array harvester experimental results by Deng et al. [14]. Deng et al. designed the five harvesters of 65 Mn spring steel with a dimension of 105 × 10 mm^2. The cantilever beams in the arrays are organized based on thickness from thinner to thicker (0.3, 0.4, 0.5, 0.6, and 0.7 mm). All the tip masses have the same mass of 10 g. All the cantilever beams are covered at the top with PVDF (polyvinylidene fluoride) piezoelectric layers at their fixed ends (see Figure 6). The dimensions of each PVDF layer are 15 × 10 mm^2 [14]. The results shown in Figure 6 obtained using FEA COMSOL are in good agreement with experimental results.

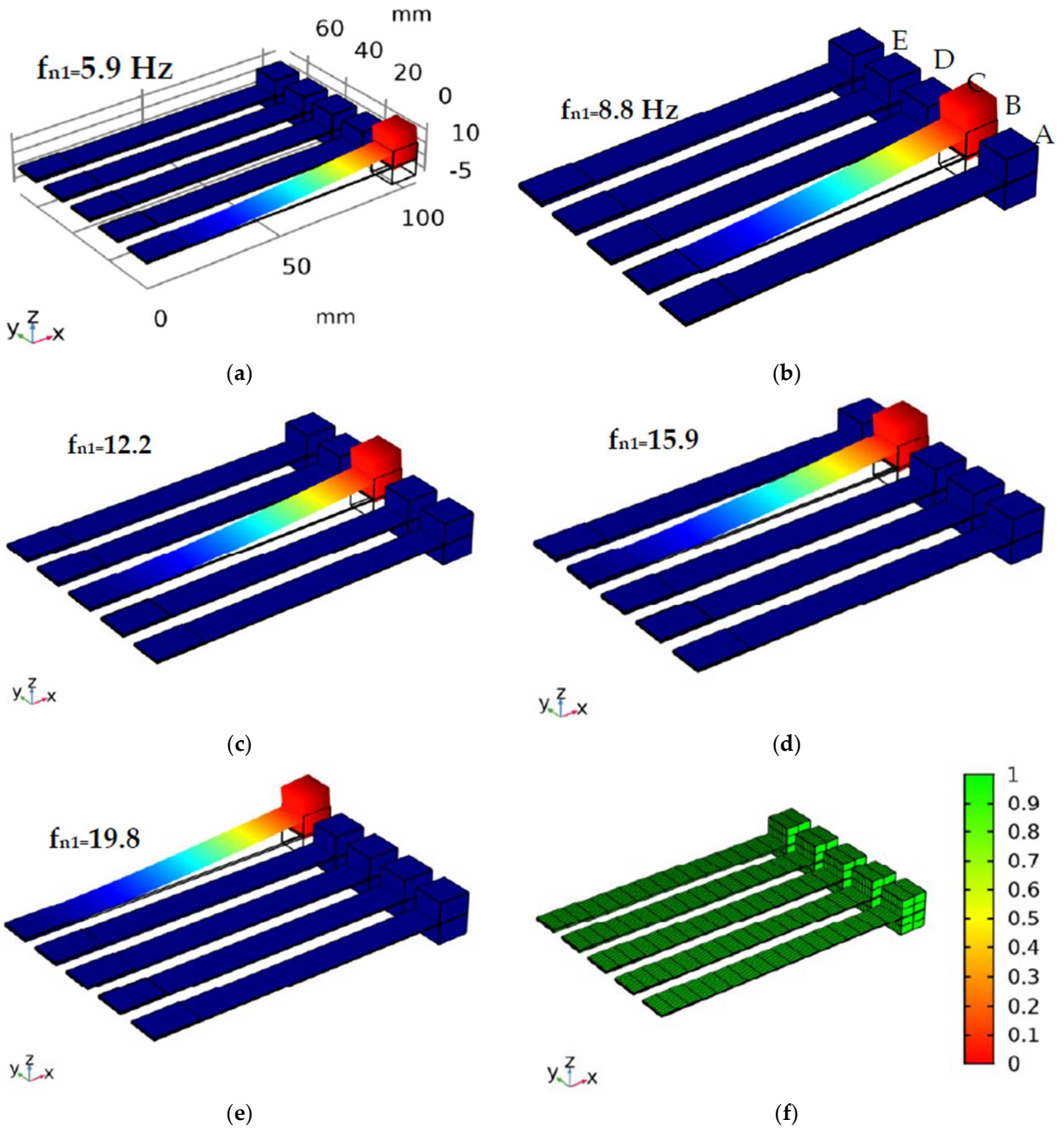

Figure 6. The natural frequencies of the second array model. (**a**) natural frequency of beam A, (**b**) natural frequency of beam B, (**c**) natural frequency of beam C, (**d**) natural frequency of beam D, (**e**) natural frequency of beam E, and (**f**) mesh accuracy of array harvester.

For the validation, the results of the analytical model are compared with those obtained from the FEM COMSOL model as shown in Figure 7. Table 4 shows the parameters utilized for this comparison. The voltage frequency response based on Equation (6) is presented in Figure 7. Figure 7 reveals good agreement between the results of the analytical model and the results of the FEA COMSOL model with an error of 2.5%.

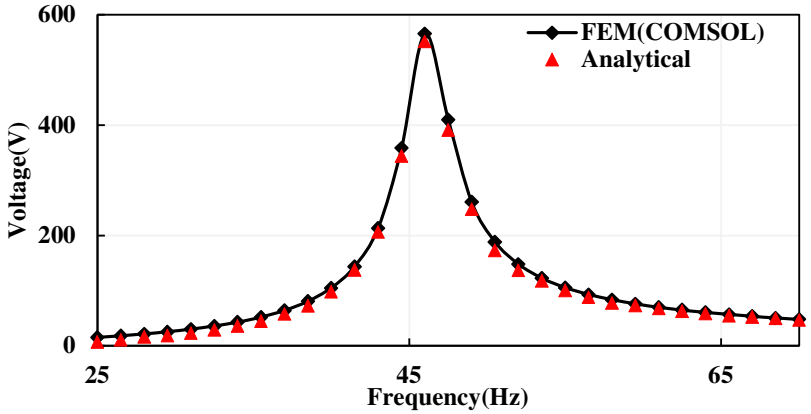

Figure 7. Voltage responses of the FEM model and the analytical model.

Table 4. Material and geometric parameters of the harvester utilized for analytical validation [40].

Parameters	Aluminum	Piezoelectric	Material	Aluminum	Piezoelectric
Length L1 + L2 (mm)	200	-	Density (kg m^{-3})	2694	7850
Length L1 (mm)	-	20	Resistance (MΩ)		10
Width b (mm)	30	30	Young's modulus (GPa)	65	59
Thickness h1 (mm)	2		Piezo. constant, e_{31} (C m^{-1})	-	−12
Thickness hp (mm)	1		Permittivity (F m^{-1})	-	1.42×10^{-8}
Thickness h2 (mm)	3		Excitation Y_b (m)	7.8×10^{-4}	
			Damping ratio	0.06	

4. ART Piezoelectric Energy Harvester Description

This section aims to design the ART harvester. The cantilever beam is designated for self-resonance fine-tuning where its natural frequency range (from 5 Hz to 22 Hz) can be controlled using the mobile mass position. Using one ART piezoelectric harvester, the five array harvesters can be replaced to give the same frequency range. The first aim is to harvest the vibration of bridges and buildings that have a frequency range of (5–22 Hz) with an excitation amplitude of (0.01–0.38 g) [39]. The frequency range can be controlled by varying the distance that the mobile mass slides through. The second objective is to optimize harvester parameters such as the piezoelectric length, piezoelectric thickness, and load resistance to maximize the output power. In addition, to study the effect of damping on the output voltage and the frequency range, high strength 65 Mn spring steel with the dimensions of 105 × 10 mm^2 and a thickness of 0.3 mm for the cantilever beam is selected along with high strength and ductility piezoelectric material (PVDF) with a width of 10 mm and length of 15 mm at fixed end. The mobile mass is made of steel with a weight of 10 g. The base excitation amplitude is 0.3 g m/s^2, which is in the excitation range of typical bridges [39]. The circuit resistance is selected to be 10 MΩ as reported by [12,14].

4.1. Automatic Resonance Tuning Mechanism Analysis

To analyze the ART mechanism, the displacement, frequency, and output voltage of the piezoelectric cantilever beam according to the mobile mass position using FEM are investigated. Figure 8a illustrates the schematic drawing of the ART energy harvester cantilever with a mobile (sliding) mass over the cantilever beam. Figure 8b shows the cross-section area of the mobile mass, where the gap below the harvester and the vibration show the mass under the displacement gradient effect. As shown in Figure 8c, the natural frequency of the proposed harvester can be modified with the movement of the sliding mass between the two stoppers. The natural frequency of the harvester increases with the movement of the mobile mass away from the free end (see Figure 8c). We utilized the two stoppers to determine the start and the end of the mass path. The two stoppers are seated at two locations (at the free end and after 70 mm from the free end). We select the

stopper locations based on the required frequency bandwidth (5–22 Hz). This frequency range lets us replace the previous harvester's array and save the material, cost, fabrication, and operation. Figure 8d shows the first natural frequency of the harvester. This model of ART energy harvester is based on the first mode only (low frequency). Figure 8e illustrates the ART technique and how the ART automatically adjusts the energy harvester's natural frequency. The natural frequency changes due to a change in the mass position, thus the change in stiffness $\left(\omega_n = \sqrt{\frac{k}{m}}\right)$. The stiffness changes according to the mass position (x_m) as follows relation $k = \frac{6EI}{x_m^2\ (1.5L - x_m)}$.

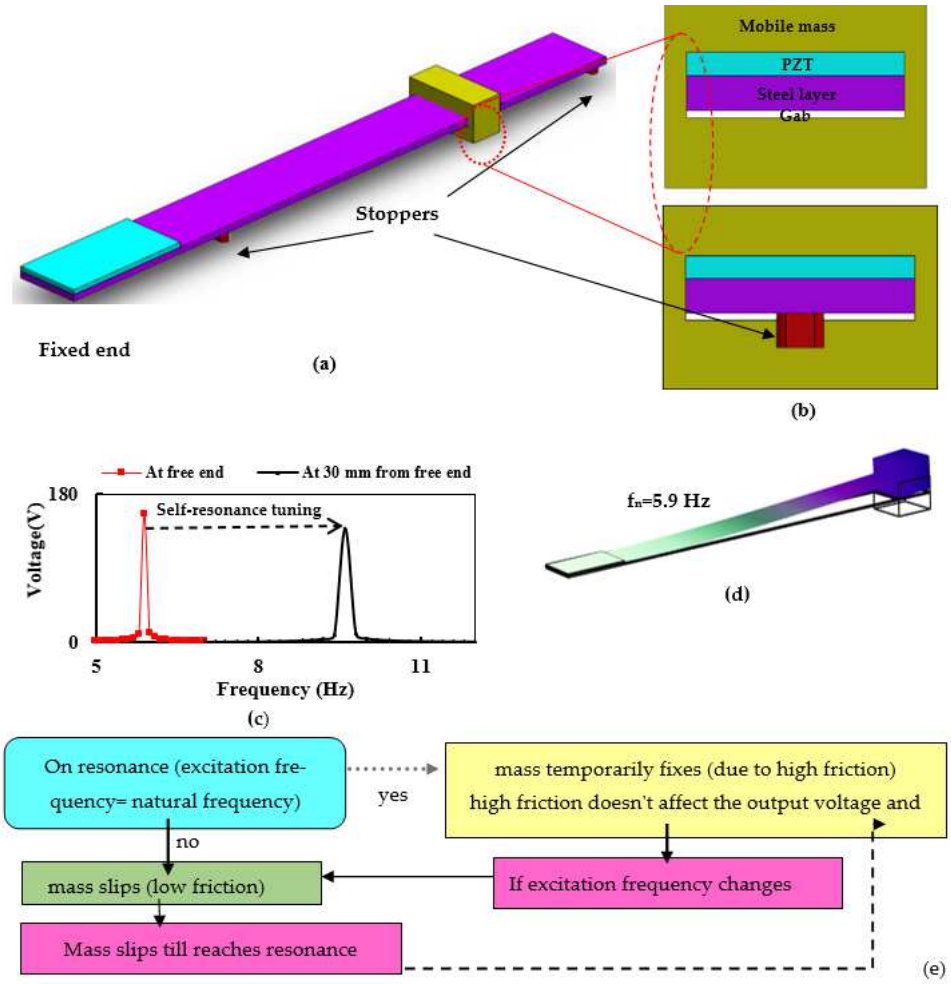

Figure 8. (**a**) Schematic diagram of the piezoelectric harvester with the mobile (sliding) mass. The natural frequency of the harvester can be tunable based on the mobile mass position, (**b**) the cross-section of the mobile mass, (**c**) self-resonance tuning using displacement difference, (**d**) first mode shape, and (**e**) flow chart of ART technique.

When the proposed harvester's base is excited, the harvester vibrates with small deflection, and the mass moves over the cantilever beam. Unlike the fixed proof mass, the mobile proof mass can move between the two stoppers due to the applied vibration. When the cantilever vibrates uniaxially at the first mode, the mobile proof mass fluctuates forth and back due to the displacement variance on both sides of the mobile mass and gab existence. At the resonance (high friction), the mass temporarily is fixed, then when the excitation frequency changes (temporarily off-resonance) (low friction), the mass slips under the displacement gradient searching for the resonance state as can be seen in Figure 8d. Thus, the motion occurs under very low friction, so the friction effect can be neglected or substituted with low damping. At the resonance (temporarily fixation), the high friction

does not affect the output voltage and power (no motion). We suggest an exact model including the friction effect in future work.

4.2. Results and Discussion

4.2.1. FEM OMSOL Simulation and Natural Frequency Mesh Convergence Study

To simulate and analyze the results of the ART piezoelectric energy harvester, we utilize the finite element method (FEM). The Eigen frequency solver and frequency domain solver are utilized to evaluate the resonance frequencies, displacement profile, mode shape, output voltage, and output power of the piezoelectric energy harvester. For extra validation and consistency, the natural frequency and maximum displacement mesh convergence to determine the optimal mesh distribution were investigated as shown in Table 5.

Table 5. The natural frequency and maximum displacement mesh convergences study.

Elements X × Elements Y	**50 × 6**	**60 × 8**	**75 × 10**	**110 × 10**	**120 × 10**
Fn_1 (Hz)	5.9	5.9	5.9	5.9	5.9
Fn_2 (Hz)	103.11	103.04	103.04	103.03	103.02
Max. disp. (mm)	4.5	4.9	5.4	6.18	6.2

4.2.2. Piezoelectric Parameters Optimization

Figure 9 shows the damping effect on the output voltage and bandwidth natural frequency. Increasing the damping ratio decreases the output voltage. Furthermore, we investigated the effect of the piezoelectric parameters such as the length and the thickness. Figure 10 reveals the effect of piezoelectric patch lengths of 10, 15, 20, and 60 mm on the output voltage and bandwidth natural frequency. Increasing the PZT length slightly increases the stiffness, natural frequency, and bandwidth natural frequency. Increasing the PZT patch length does not always enhance the output voltage and output power.

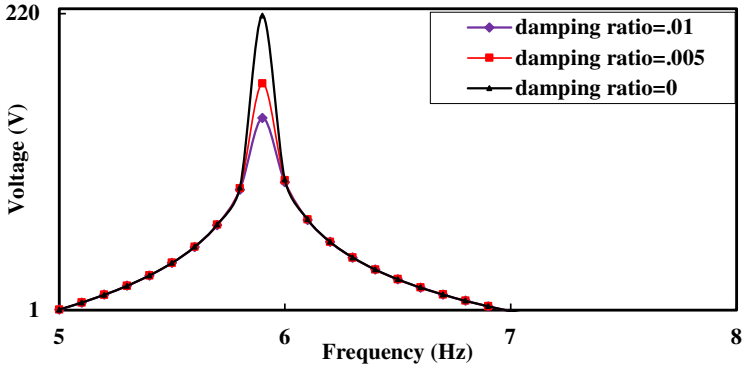

Figure 9. The effect of the damping ratio on the output voltage.

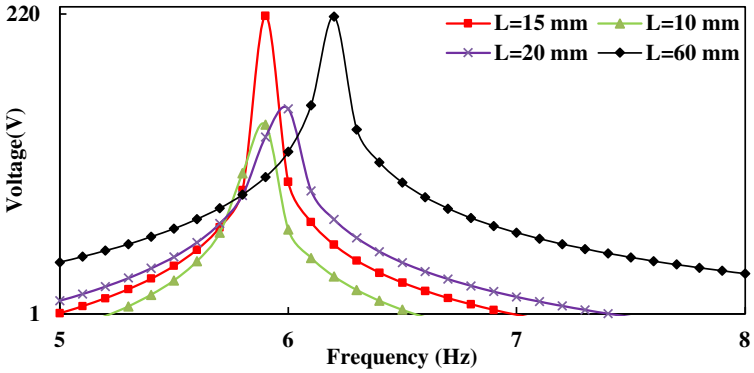

Figure 10. The effect of the PZT length on the output voltage and bandwidth natural frequency.

This greatly depends on the electromechanical coupling coefficient $k^2 = \frac{\theta^2}{k_h\ c_p}$ that was previously s defined in this paper and also depends on the capacitance and the stiffness. Furthermore, the PZT is more effective besides the fixed end (high strain) and less effective at the free end. However, the capacitance quite increases linearly with the added piezoelectric length from the following relation $c_p = \frac{e_{33}^s b\ L_1}{h_p}$, so increasing the length increases the capacitance and decreases the electromechanical coupling coefficient. For previous reasons and justifications, increasing the piezoelectric length does not always give more voltage. The optimal piezoelectric length obtained is 15 mm which produces 213 V and 2.28 mW. Figure 11 shows that the optimal PZT thickness is 0.3 mm. also. We found that increasing the PZT thickness increases the frequency and does not always increase the output voltage and output power. It depends on the capacitance and stiffens as mentioned in the previous relations.

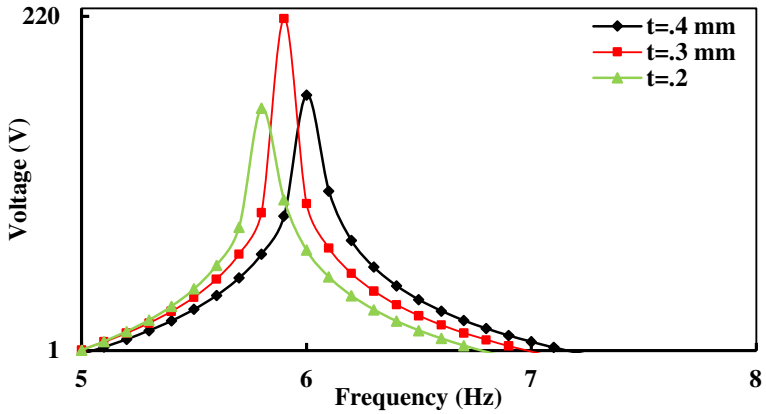

Figure 11. The effect of the PZT thickness on the output voltage and bandwidth natural frequency.

4.2.3. ART Piezoelectric Energy Harvester Investigation

To recognize the ART mechanism of the piezoelectric cantilever harvester with the mobile mass, the displacement profile along the cantilever according to the mass location is plotted. Figure 12 shows the FEM-simulated displacement profile of the harvester and its natural frequencies when the mass is at the free end, 30 mm, 50 mm, 60 mm, and 70 mm from the free end. When the mobile mass is at the free end, the displacement decreases from 6.2 mm at the free end to 0 at the fixed end (see Figure 12a). When the mobile mass moves away from the free end, the maximum displacement decreases and the natural frequency increases, and the output voltage decreases. Table 6 shows that the natural frequency increases as the mobile mass moves away from the free end. The results of Table 6 are plotted in Figure 13. From the results shown in Figure 13 and Table 6, we can find a relationship between the mass position from the free end (x_m) and the natural frequency. Using the polyfit MATLAB function and the curve-fitting option, we can find the polynomial relationship between the frequency and mass position. Using this relation, we can determine the frequency at any mass position. This relation can be expressed as:

$$\text{Resonance frequency (Hz)} = 5.9 + 0.944x_m + 125 * 10^{-6}x_m^2 + 41 * 10^{-6}x_m^3 - 178 * 10^{-6}x_m^4 \quad (20)$$

Table 6. The natural frequency of the harvester at different mass positions.

Mass Position from the Free End (x_m mm)	**0**	**30**	**50**	**60**	**70**
Frequency (Hz)	5.9	9.6	14.36	17.8	21.9

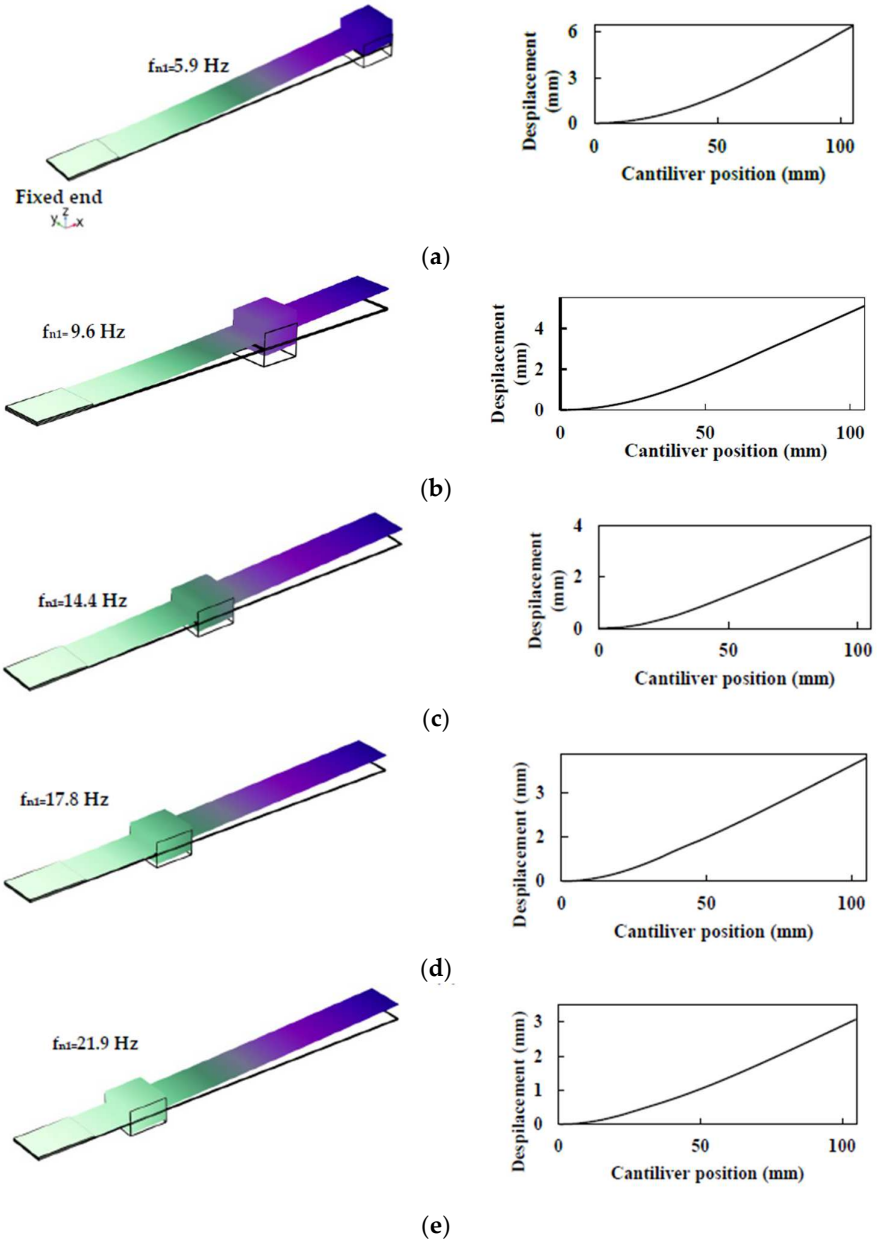

Figure 12. Simulated displacement profile and natural frequency of the ART energy harvester based on mass positions. The mobile mass is located at (**a**) 0 mm (at the free end), (**b**) 30 mm, (**c**) 50 mm, (**d**) 60 mm, and (**e**) 70 mm from the free end of the cantilever.

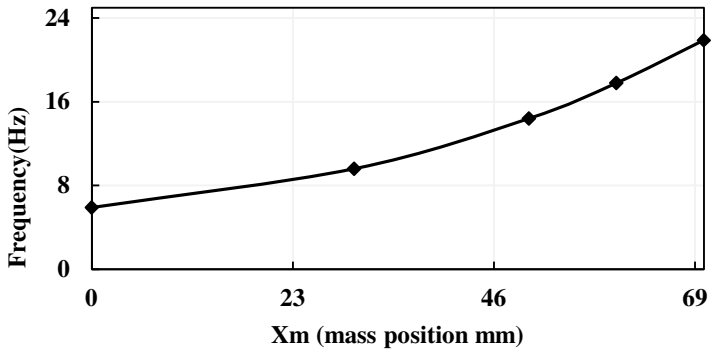

Figure 13. Relationship between the natural frequency and the mass position x_m (mm) measured from the free end.

Figure 14 shows the output voltage when the mass is at the free end, 30 mm, 50 mm, 60 mm, and 70 mm from the free end, respectively. Figure 14 reveals that the voltage decreases as the mass slides away from the free end due to the decreasing of the mobile mass bending stress whereas the bandwidth natural frequency increases. Figure 15 shows the resonance frequency tuning range of the ART energy harvester compared with the fixed proof masses. Figure 13 plots the mass position against frequency. Figure 15 plots the frequency with the output voltage, so the relation between the mass position and voltage can be deduced. The bandwidths for the ART harvester and the fixed mass harvester are found to be 17 Hz and 1.5 Hz, respectively. The bandwidth of the ART energy harvester is 11.3 times the bandwidth of the conventional energy harvester (this enhancement is due to the proposed design). Figure 16 shows the frequency response of the output power of the piezoelectric harvester at two positions of mass. The equation of output power, utilized in COMSOL modeling for all cases in this paper, is derived by Lefeuvre et al. [44]. This equation is expressed as:

$$\text{Power} = \text{v}\left(\frac{2\alpha_2}{\frac{\pi}{2} + R_l \text{c}_\text{p} \omega_\text{n}} + c_v \frac{\frac{\pi}{2} + R_l \text{c}_\text{p} \omega_\text{n}}{\alpha_2 R_l}\right) \tag{21}$$

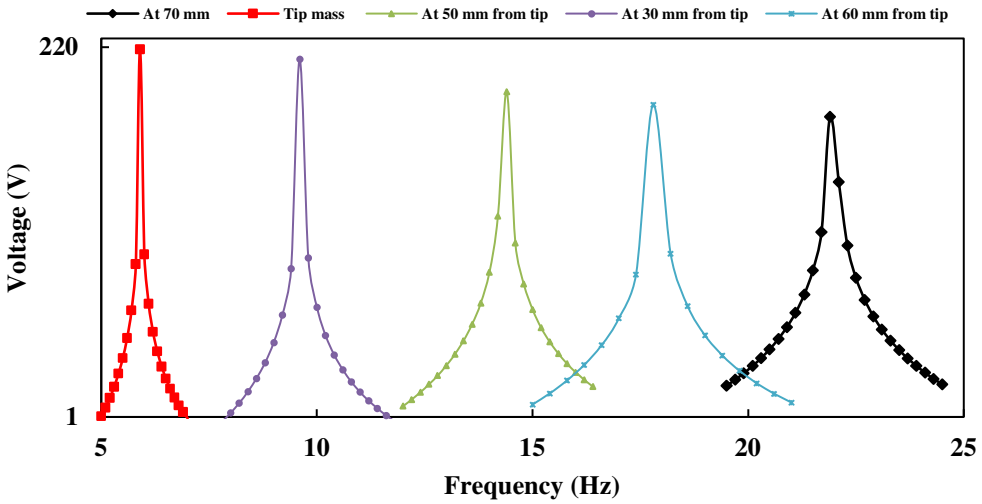

Figure 14. The voltage of the harvester at different frequencies.

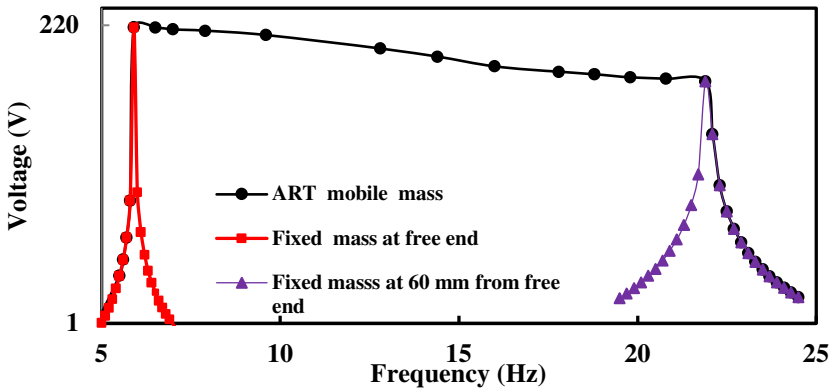

Figure 15. The resonance frequency tuning range of ART energy harvester compared with the fixed proof masses.

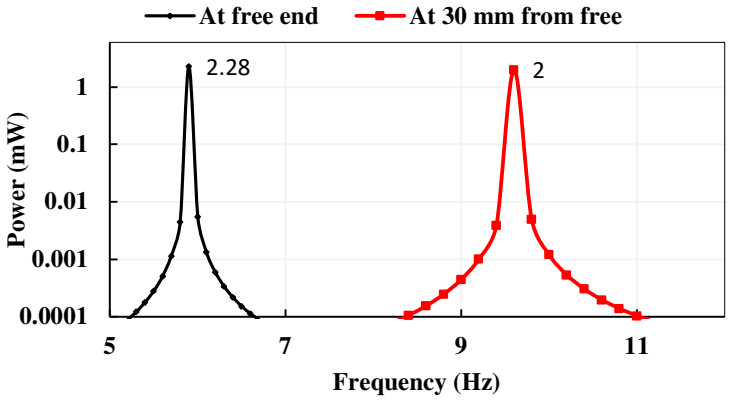

Figure 16. The frequency response of the output power of the piezoelectric harvester at two positions for the mobile mass.

4.2.4. Performance of the Proposed Design

In this section, we compare our proposed broadband technique with similar designs. The most used system of measurement and fair for energy harvesters is the power density [1], which is equal to the power output per active volume. Therefore, in this section, we use the power density to compare the other techniques with the proposed technique. Table 7 compares the performance of our technique with related techniques based on the power density. Additionally, the frequency range of each design is included. The utilized piezoelectric material also affects the performance, so it is included in the comparison. Based on the properties listed by reference [1], the PVDF is the lowest performance among the piezoelectric materials, but it is a ductile material. Based on the results listed in Table 7, our proposed technique gives the best performance with a power density of 0.05 mW mm^{-3} and a frequency range of 17 Hz. It is observed that the output power is increased from 2.28 to 52.4 due to the resistance optimization (see next section). It is observed that the improvement provided by our technique in the frequency range and the power density is due to the optimization of the parameters and design. Table 8 shows the comparison of the ART broadband technique with other techniques. Moreover, this technique gives more broadband natural frequency than the other techniques. Employing the proposed techniques saves time, cost, and effort because this technique does not require a sensor, actuator, magnet, stopper, or spring.

Table 7. Performance Comparison of the proposed techniques with related techniques.

Ref.	Technique	Piezoelectric Material	Excitation; g = 9.8 m/s^2	Frequency Range (Hz)	Piezo Size (mm^3) × Number	Mass (g)	Power	Power Density (mW/mm^3)
This study	ART	PVDF	0.3 g	5–22	(15 × 10 × 0.3)	10 g	2.28 mW	0.05
[11]	bistable	PZT	0.5 g	3–13	(26.2 × 3.8 × 0.25)	-	1.3 mW	0.05
[12]	array	MFC	2 g	10–13.4	(38 × 17 × 0.3 × 4)	45 g	1.35 mW	0.0017
[15]	Active resonance	PZT	5 V	66–89	(40 × 11 × 0.6 × 2)		30 µW	0.05 × 10^{-3}
[31]	Mass tuning array	PVDF	3.5 mm	19–29	(15 × 10 × 0.3 × 5)	40 g	2.5 mW	0.011
[26]	centrifugal softening	PZT-5H	3.5 g	8–14	(25 × 12 × 0.15)		0.3 mW	0.006
[45]	-	PZT	0.5 g	56	5918.9	100	4.76 µW	0.804 × 10^{-6}
[46]	-	PZT	0.25 g	68	0.11	5	0.023	0.209 × 10^{-3}
[8]	-	PZT	3.5 g	75	(4 × 3.5 × 1 × 4)	7.8	0.239	4.27 × 10^{-6}

Table 8. Comparison of the ART broadband technique with other techniques.

Technique	Disadvantageous
ART energy harvester	Fatigue stress due to the changing load of mass needs to be investigated.
External magnetic [9–11]	Need for external magnet and mass; additionally, need for controlling the distance between the fixed mass and moving magnet.
Array harvester [12–14]	Large dimensions, high weight, many components, and a small improvement in bandwidth.
Active resonance tuning [15]	Need for sensors and actuators and low net output power.
External magnetic [9–11]	Need for external magnet and mass; additionally, need for controlling the distance between the fixed mass and moving magnet.

We must consider the following factors that cause the loss in the harvester: (1) dielectric loss, (2) low electromechanical coupling, (3) working away from resonance, (4) small vibration source frequency, and (5) power-boosting interface. The first three factors must be decreased in our optimal design. In contrast, the fourth factor is required in many practical situations to match the ambient vibration frequency. Whereas the fifth factor is desired to increase the power density of the system, the last two factors must meet the practical with the minimum total loss [47]. The effect of dielectric loss should be studied for excitation, material, and structure to accurately evaluate the output power [47]. Investigation of the efficiency and the loss in the system is a vital feature that must be considered in future work.

4.2.5. Power Optimization

The load resistance R_l is optimized in the circuit to maximize the output power of the piezoelectric energy harvester. The load circuit resistance is assigned by 10^7 Ω based on the recommendation of Deng et al. [14]. However, the resistance optimization highly maximizes the output power. For the same dimensions used in this study and using the resistance dependence of the power, it is found that the optimal resistance is 5×10^8 Ω and optimal power output is 52.4 mW. The power improves from 2.2 mW at 10^7 Ω to 52.4 at 5×10^8 Ω (see Figure 17). The power optimization based on the PZT length, PZT thickness, and load resistance highly improves the output power. Figure 16 shows the resistance dependence of power and voltage. Figure 18 shows the acceleration dependence of power and voltage in the range of (0.01–0.35 g). Increasing the acceleration increases output voltage and output power due to increasing the vibrations and induced stresses.

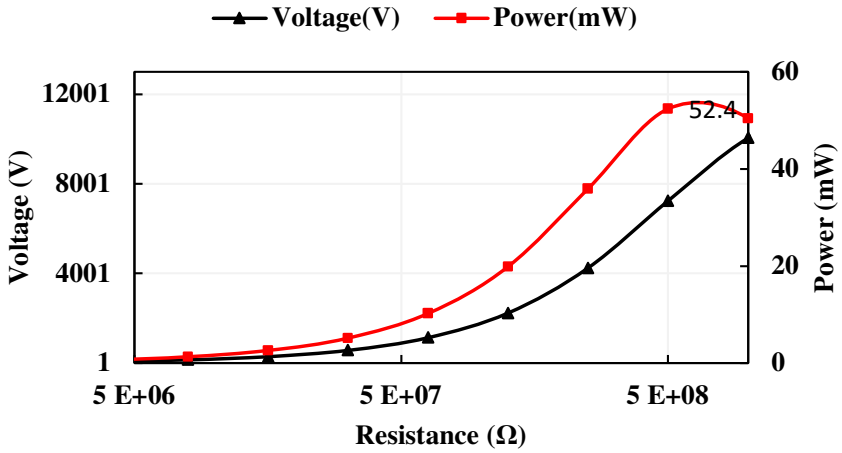

Figure 17. The resistance dependence of power and voltage.

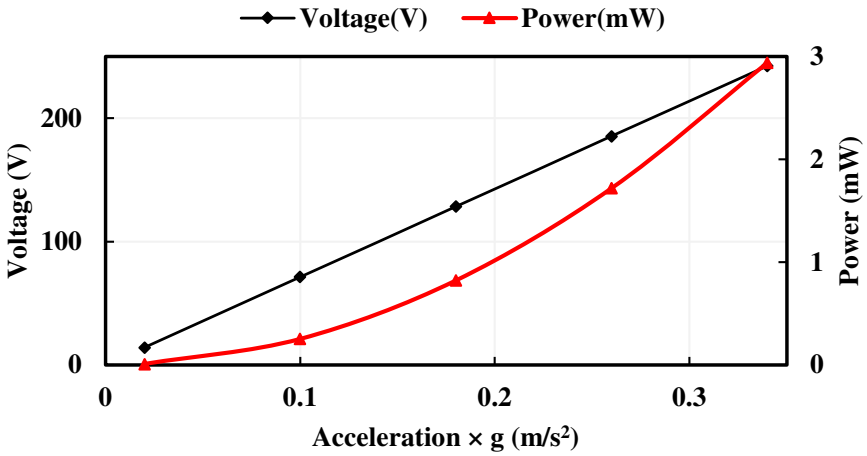

Figure 18. The acceleration dependence of power and voltage.

5. Conclusions

In this paper, it was demonstrated that automatic resonance tuning (ART) piezoelectric energy harvester is capable of giving broad bandwidth natural frequency using the sliding motion of the mobile proof mass. The ART energy harvester design consists of a piezoelectric cantilever beam with a mobile mass by a small gap between the mass and beam. The high friction at resonance lets the mass stop and low friction at off-resonance cause the mass to move (ART phenomenon). Modification of the natural frequency of the ART piezoelectric energy harvester was demonstrated according to the mass position. Furthermore, we demonstrated the output voltage and displacement profile of the harvester numerically using FEM at different mass positions. An optimization process was performed by selecting the optimal PZT dimensions and optimal resistance to maximize the output voltage and output power. The bandwidth of the ART energy harvester's natural frequency was broadening to 1130% of the conventional resonance energy harvester. It was observed that our proposed broadband design gave the best performance compared with similar techniques with a power density of 0.05 mW mm^{-3} and frequency range (5–22) Hz. The maximum recorded output power (without optimization) was 2.28 mW whereas the maximum recorded output power (with resistance optimization) was 52.4 mW. The results of the FEM were validated using the analytical results. In addition, the model was validated using three literature results of both single harvester and array harvesters, and it was found that the error was around 2%.

6. Future work

The proposed automatic resonance tuning (ART) piezoelectric energy harvester provides high output power through broadband natural frequency. It is recommended in future work to analytically investigate the ART model (moving mass). Furthermore, it is recommended to include friction in this investigation, and an array of ART beams can be modeled.

Author Contributions: S.A.K., was responsible for the establishing and applying the new methodology introduced in this work. S.A.K. and M.A.B.-H. worked closely to derive the analytical and numerical models presented in this work. Both the derivations and statistical methods were closely tested and confirmed by S.A.K., M.A.B.-H., M.M.Y.B.E. and W.A.A. who suggested the procedures that were utilized. M.M.Y.B.E. and W.A.A. provided his expertise and technical background in composite materials and assisted S.A.K. with carrying out the numerical analyses and implementation of algorithm. M.A.B.-H., M.M.Y.B.E., M.B. and W.A.A. worked closely with S.A.K. in the reviewing and editing phase. All authors have read and agreed to the published version of the manuscript.

Funding: This research received no external funding.

Data Availability Statement: This research received no Data Availability Statement.

Acknowledgments: Authors would like to thank the Smart critical infrastructure research Centre -High performance Computer Lab, Alexandria University, Egypt for providing the facility to perform the simulation of this study.

Conflicts of Interest: The authors declare no conflict of interest.

References

1. Yang, Z.; Zhou, S.; Zu, J.; Inman, D. High-Performance Piezoelectric Energy Harvesters and Their Applications. *Joule* **2018**, *2*, 642–697. [CrossRef]
2. Safaei, M.; Sodano, H.A.; Anton, S.R. A review of energy harvesting using piezoelectric materials: State-of-the-art a decade later (2008–2018). *Smart Mater. Struct.* **2019**, *28*, 113001. [CrossRef]
3. Priya, S.; Song, H.C.; Zhou, Y.; Varghese, R.; Chopra, A.; Kim, S.G.; Kanno, I.; Wu, L.; Ha, D.S.; Ryu, J. A review on piezoelec-tric energy harvesting: Materials, methods, and circuits. *Energy Harvest. Syst.* **2017**, *4*, 3–39. [CrossRef]
4. Yang, B.; Lee, C.; Xiang, W.; Xie, J.; He, J.H.; Kotlanka, R.K.; Low, S.P.; Feng, H. Electromagnetic energy harvesting from vi-brations of multiple frequencies. *J. Micromech. Microeng.* **2009**, *19*, 035001. [CrossRef]
5. Crovetto, A.; Wang, F.; Hansen, O. Modeling and Optimization of an Electrostatic Energy Harvesting Device. *J. Microelectromech. Syst.* **2014**, *23*, 1141–1155. [CrossRef]
6. Bowen, C.R.; Kim, H.A.; Weaver, P.M.; Dunn, S. Piezoelectric and ferroelectric materials and structures for energy harvesting applications. *Energy Environ. Sci.* **2013**, *7*, 25–44. [CrossRef]
7. Maurya, D.; Kumar, P.; Khaleghian, S.; Sriramdas, R.; Kang, M.G.; Kishore, R.; Kumar, V.; Song, H.-C.; Park, J.-M.; Taheri, S.; et al. Energy harvesting and strain sensing in smart tire for next generation autonomous vehicles. *Appl. Energy* **2018**, *232*, 312–322. [CrossRef]
8. Song, H.C.; Kumar, P.; Maurya, D.; Kang, M.G.; Reynolds, W.T.; Jeong, D.Y.; Kang, C.-Y.; Priya, S. Ultra-low resonant piezoe-lectric MEMS energy harvester with high power density. *J. Microelectromech. Syst.* **2017**, *26*, 1226–1234. [CrossRef]
9. Cottone, F.; Vocca, H.; Gammaitoni, L. Nonlinear Energy Harvesting. *Phys. Rev. Lett.* **2009**, *102*, 080601. [CrossRef]
10. Arrieta, A.F.; Hagedorn, P.; Erturk, A.; Inman, D.J. A piezoelectric bistable plate for nonlinear broadband energy harvesting. *Appl. Phys. Lett.* **2010**, *97*, 104102. [CrossRef]
11. Stanton, S.C.; McGehee, C.C.; Mann, B.P. Nonlinear dynamics for broadband energy harvesting: Investigation of a bistable piezoelectric inertial generator. *Phys. Nonlinear Phenom.* **2010**, *239*, 640–653. [CrossRef]
12. TYildirim, T.; Zhang, J.; Sun, S.; Alici, G.; Zhang, S.; Li, W. Design of an enhanced wideband energy harvester using a paramet-rically excited array. *J. Sound Vib.* **2017**, *410*, 416–428. [CrossRef]
13. Song, H.-C.; Kumar, P.; Sriramdas, R.; Lee, H.; Sharpes, N.; Kang, M.-G.; Maurya, D.; Sanghadasa, M.; Kang, H.-W.; Ryu, J.; et al. Broadband dual phase energy harvester: Vibration and magnetic field. *Appl. Energy* **2018**, *225*, 1132–1142. [CrossRef]
14. Deng, H.; Du, Y.; Wang, Z.; Ye, J.; Zhang, J.; Ma, M.; Zhong, X. Poly-stable energy harvesting based on synergetic multista-ble vibration. *Commun. Phys.* **2019**, *2*, 2–21. [CrossRef]
15. Peters, C.; Maurath, D.; Schock, W.; Mezger, F.; Manoli, Y. A closed-loop wide-range tunable mechanical resonator for energy harvesting systems. *J. Micromech. Microeng.* **2009**, *19*, 094004. [CrossRef]
16. Lu, C.; Tsui, C.-Y.; Ki, W.-H. Vibration Energy Scavenging System with Maximum Power Tracking for Micropower Applications. *IEEE Trans. Very Large Scale Integr. Syst.* **2010**, *19*, 2109–2119. [CrossRef]
17. Mohamed, K.; Elgamal, H.; Kouritem, S.A. An experimental validation of a new shape optimization technique for piezoelectric harvesting cantilever beams. *Alex. Eng. J.* **2020**, *60*, 1751–1766. [CrossRef]
18. Wang, X.; Xia, Y.; Shi, G.; Xia, H.; Chen, M.; Chen, Z.; Ye, Y.; Qian, L. A Novel MPPT Technique Based on the Envelope Extrac-tion Implemented with Passive Components for Piezoelectric Energy Harvesting. *IEEE Trans. Power Electron.* **2021**, *36*, 12685–12693. [CrossRef]
19. Kouritem, S.A.; Elshabasy, M.M. Tailoring the panel inertial and elastic forces for the flutter and stability characteristics enhance-ment using copper patches. *Compos. Struct.* **2021**, *274*, 114311. [CrossRef]
20. Elshabasy, M.M.; Kouritem, S.A. Thickening of optimally selected locations on panels subjected to unyawed flow for substantial delay of the panel flutter. *Alex. Eng. J.* **2020**, *59*, 5031–5044. [CrossRef]
21. Kouritem, S.A.; Elshabasy, M.M.Y.B.; El-Gamal, H.A. Optimum Location/Area of PZT Actuators for Flutter Damping Using Norm Feedback Control Gain-Based Iterative Method. In Proceedings of the 2015 World Congress on Advances in Structural Engineering and Mechanics (ASEM15), Incheon, Korea, 25–29 August 2015.
22. Kouritem, S.A.; Elshabasy, M.M.Y.B.; El-Gamal, H.A. FE Meshing Scheme for Accurate Placement/Area of PZT Actuators for Flutter Damping Using LQR Method. In Proceedings of the 2015 World Congress on Advances in Structural Engineering and Mechanics (ASEM15), Incheon, Korea, 25–29 August 2015; Available online: https://www.researchgate.net/publication (accessed on 30 July 2022).
23. Kouritem, S.A.; Abouheaf, M.I.; Nahas, N.; Hassan, M. A multi-objective optimization design of industrial robot arms. *Alex. Eng. J.* **2022**, *61*, 12847–12867. [CrossRef]
24. Jian, Y.; Tang, L.; Hu, G.; Li, Z.; Aw, K.C. Design of graded piezoelectric metamaterial beam with spatial variation of electrodes. *Int. J. Mech. Sci.* **2022**, *218*, 107068. [CrossRef]

25. Wang, Z.; Du, Y.; Li, T.; Yan, Z.; Tan, T. A flute-inspired broadband piezoelectric vibration energy harvesting device with me-chanical intelligent design. *Appl. Energy* **2021**, *303*, 117577. [CrossRef]
26. Li, M.; Jing, X. Novel tunable broadband piezoelectric harvesters for ultralow-frequency bridge vibration energy harvesting. *Appl. Energy* **2019**, *255*, 113829. [CrossRef]
27. Staaf, L.G.H.; Smith, A.D.; Lundgren, P.; Folkow, P.D.; Enoksson, P. Effective piezoelectric energy harvesting with bandwidth en-hancement by asymmetry augmented self-tuning of conjoined cantilevers. *Int. J. Mech. Sci.* **2018**, *150*, 1–11. [CrossRef]
28. Rui, X.; Zeng, Z.; Zhang, Y.; Li, Y.; Feng, H.; Huang, X.; Sha, Z. Design and experimental investigation of a self-tuning piezoelectric energy harvest-ing system for intelligent vehicle wheels. *IEEE Trans. Veh. Technol.* **2020**, *69*, 1440–1451. [CrossRef]
29. Kim, H.; Tai, W.C.; Parker, J.; Zuo, L. Self-tuning stochastic resonance energy harvesting for rotating systems under modulated noise and its application to smart tires. *Energy Convers. Manag.* **2019**, *122*, 769–785. [CrossRef]
30. Kouritem, S.A. Array of piezoelectric energy harvesters for broadband natural frequency applications. In Proceedings of the ICSV27, Annual Congress of International Institute of Acoustics and Vibration (IIAV), Prague, Czech Republic, 11–16 July 2021.
31. Kouritem, S.A.; Al-Moghazy, M.A.; Noori, M.; Altabey, W.A. Mass tuning technique for a broadband piezoelectric energy harvester array. *Mech. Syst. Signal Process.* **2022**, *181*, 109500. [CrossRef]
32. Silveira, A.; Danie, G. Optimization analysis of an energy harvester for smart tilting pad journal bearings considering higher vibration modes. *Mech. Syst. Signal Process.* **2022**, *166*, 108404. [CrossRef]
33. Liu, C.; Liao, B.; Zhao, R.; Yu, K.; Lee, H.P.; Zhao, J. Large Stroke tri-stable vibration energy harvester: Modelling and experimental vali-dation. *Mech. Syst. Signal Process.* **2022**, *168*, 108699. [CrossRef]
34. Babitsky, V.; Veprik, A. Damping of Beam Forced Vibration By A Moving Washer. *J. Sound Vib.* **1993**, *166*, 77–85. [CrossRef]
35. Thomsen, J.J. Vibration suppression by using self-arranging mass: Effects of adding restoring force. *J. Sound Vib.* **1996**, *197*, 403–425. [CrossRef]
36. Miller, L.M.; Pillatsch, P.; Halvorsen, E.; Wright, P.K.; Yeatman, E.M.; Holmes, A.S. Experimental passive self-tuning behavior of a beam resonator with sliding proof mass. *J. Sound Vib.* **2013**, *332*, 7142–7152. [CrossRef]
37. Fan, Z.; Islam, N.; Bayne, S.B. Towards kilohertz electrochemical capacitors for filtering and pulse energy harvesting. *Nano Energy* **2017**, *39*, 306–320. [CrossRef]
38. Li, H.; Tian, C.; Deng, Z.D. Energy harvesting from low frequency applications using piezoelectric materials. *Appl. Phys. Rev.* **2014**, *1*, 041301. [CrossRef]
39. Khan, F.; Ahmad, I. Review of Energy Harvesters Utilizing Bridge Vibrations. *Shock Vib.* **2015**, *2016*, 1–21. [CrossRef]
40. Lee, C.; Lin, J. Incorporating piezoelectric energy harvester in tunable vibration absorber for application in multi-modal vibra-tion reduction of a platform structure. *J. Sound Vib.* **2017**, *389*, 73–88. [CrossRef]
41. Dutoit, N.E.; Wardle, B.L.; Kim, S. Design considerations for MENMS-scale piezoelectric mechanical vibration energy harvest-ers. *J. Integr. Ferroelectr.* **2005**, *71*, 121–160. [CrossRef]
42. Jasem, M.H. Study the effect of the variation of layer's thickness on the bending characteristics of the composite beam. *Al-Qadisiya J. Eng. Sci.* **2012**, *5*, 354–366.
43. Shin, Y.-H.; Choi, J.; Kim, S.J.; Kim, S.; Maurya, D.; Sung, T.-H.; Priya, S.; Kang, C.-Y.; Song, H.-C. Automatic resonance tuning mechanism for ultra-wide bandwidth mechanical energy harvesting. *Nano Energy* **2020**, *77*, 104986. [CrossRef]
44. Lefeuvre, E.; Audigier, D.; Richard, C.; Guyomar, D. Buck-Boost Converter for Sensorless Power Optimization of Piezoelectric Energy Harvester. *IEEE Trans. Power Electron.* **2007**, *22*, 2018–2025. [CrossRef]
45. Wu, J.; Chen, X.; Chu, Z.; Shi, W.; Yu, Y.; Dong, S. A barbell-shaped high-temperature piezoelectric vibration energy har-vester based on $BiScO_3$-$PbTiO_3$, ceramic. *Appl. Phys. Lett.* **2016**, *109*, 173901. [CrossRef]
46. Hung, C.F.; Chung, T.K.; Yeh, P.C.; Chen, C.C.; Wang, C.M.; Lin, S.H. A miniature mechanical-piezoelectricconfigured three-axis vibrational energy harvester. *IEEE Sens. J.* **2015**, *15*, 5601–5615. [CrossRef]
47. Liang, J.; Chung, H.S.H.; Liao, W.H. Dielectric loss against piezoelectric power harvesting. *Smart Mater. Struct.* **2014**, *23*, 092001. [CrossRef]